*Progress In Electromagnetics Research, Vol. 133, 495–513, 2013*

# THE USE OF A HUMAN BODY MODEL TO DETERMINE THE VARIATION OF PATH LOSSES IN THE HUMAN BODY CHANNEL IN WIRELESS CAPSULE ENDOSCOPY

**M. R. Basar[1, *], F. Malek[2], K. M. Juni[3], M. I. M. Saleh[3], M. S. Idris[3], L. Mohamed[2], N. Saudin[2], N. A. Mohd Affendi[2], and A. Ali[2]**

[1]School of Computer and Communication Engineering, Universiti Malaysia Perlis (UniMAP), Taman Seberang Jaya Fasa 3, Kuala Perlis, Perlis 02000, Malaysia

[2]School of Electrical System Engineering, Universiti Malaysia Perlis (UniMAP), Pauh Putra, Arau, Perlis 02600, Malaysia

[3]Electrical Engineering Department, PoliteknikTuanku Syed Sirajuddin (PTSS), Pauh Putra, Perlis 02600, Malaysia

**Abstract**—Presently, wireless capsule endoscopy (WCE) is the sole technology for inspecting the human gastrointestinal (GI) tract for diseases painlessly and in a non-invasive way. For the further development of WCE, the main concern is the development of a high-speed telemetry system that is capable of transmitting high-resolution images at a higher frame rate, which is also a concern in the use of conventional endoscopy. A vital task for such a high-speed telemetry system is to be able to determine the path loss and how it varies in a radio channel in order to calculate the proper link budget. The hostile nature of the human body's channel and the complex anatomical structure of the GI tract cause remarkable variations in path loss at different frequencies of the system as well as at capsule locations that have high impacts on the calculation of the link budget. This paper presents the path loss and its variation in terms of system frequency and location of the capsule. Along with the guideline about the optimum system frequency for WCE, we present the difference between the maximum and minimum path loss at different anatomical regions, which is the most important information in the link-margin setup for highly efficient telemetry systems in next-generation capsules. In order

*Received 12 September 2012, Accepted 30 October 2012, Scheduled 6 November 2012*

* Corresponding author: Md. Rubel Basar (rubel24434@yahoo.com).

to investigate the path loss in the body's channel, a heterogeneous human body model was used, which is more comparable to the human body than a homogenous model. The finite integration technique (FIT) in Computer Simulation Technology's (CST's) Microwave Studio was used in the simulation. The path loss was analyzed in the frequency range of 100 MHz to 2450 MHz. The path loss was found to be saliently lower at frequencies below 900 MHz. The smallest loss was found around the frequency of 450 MHz, where the variation of path loss throughout the GI tract was 29 dB, with a minimum of −9 dB and a maximum of −38 dB. However, at 900 MHz, this variation was observed to be 38 dB, with a minimum of −10 dB and a maximum of −48 dB. For most positions of the capsule, the path loss increased rapidly after 900 MHz, reaching its peak at frequencies in the range of 1800 MHz to 2100 MHz. During examination of the lower esophageal region, the maximum peak observed was −84 dB at a frequency of 1760 MHz. The path loss was comparatively higher during examination of anatomically-complex regions, such as the upper intestine and the lower esophagus as compared to the less complex stomach and upper esophagus areas.

## 1. INTRODUCTION

The invention of wireless capsule endoscopy (WCE) [1] brought about the greatest revolution in the technology used to diagnose GI problems, because it eliminated the acute pain and discomfort associated with the use of conventional push endoscopy to examine the GI tract. In this novel system, a pill-sized electronic capsule that contains image acquisition and telemetry systems, along with a battery as the power source [2], passes through the patient's GI tract and transmit real-time images to the lead antenna that is connected to the image-receiving box, which is outside of the body [3].

The main issues that must be overcome if there is to be wider clinical applications of WCE are poor-quality images, a low image-transmission rate, and the localization of the capsule. High-quality transmission of images requires an efficient telemetry system, acceptable condition of the channel (between the capsule and the receiving antenna), and consideration of the system-link budget. The amount of signal attenuation during radio propagation, i.e., path loss, characterizes the condition of the channel [4–6]. In this regard, the system's frequency and the calculation of the proper link budget have greater influence on the system's performance [7–9]. Unfortunately, most of the research related to the WCE's telemetry system has conducted with the random selection of the system's frequency without

proper consideration of the propagation characteristics of the human body on the system's frequency [10]. In light of that, the following upgrades to the capsule-endoscopy system have been proposed: a low-power, 3–5-GHz,ultra-wideband transceiver [11]; a 15-Mbps, 900-MHz ASK transmitter [12]; a 2.4-GHz, high-data-rate transceiver [13]; a 0.5-GHz, high-speed, high-efficiency system [14]; a 1.4-GHz conformal, ingestible, capsule antenna [15]; and a 2.4-GHz, peanut-shaped, printed antenna for the bio-telemetric tablet [16].

However, the human body is a complex composite of many different tissues that are highly-dependent on frequency. The conductivity and relative permittivity of these tissues vary with frequency [17–19] and age group [20, 21], resulting in propagation characteristics that differ according to the anatomical region, e.g., esophagus, stomach, and upper and lower intestines, depending on the depth of the device in the body. In the open literature, there are many publications that address modelling of the human body's channel for wireless body area network (WBAN). A few of the publication addressed communication with the instrument inside the body, but very few research studies focused specifically on WCE. The radiation from the ingested capsule in the human intestine was tested in the frequency range of 150 MHz to 1200 MHz, and it was observed that the maximum radiation was between 450 MHz and 900 MHz and that more radiation occurred in the anterior region than in the posterior region [22]. The propagation of the electromagnetic field from the intestine was investigated for the range of frequencies from 100 MHz to 700 MHz using the homogenous model of the body and the heterogeneous model, and two unusual behaviours were observed, i.e., relatively lower attenuation above 400 MHz and dip radiation at frequencies less than 400 MHz [23]. The depth of capsule device is a very important factor that affects path loss and that, for WCE, varies from patient to patient. A parallel finite-difference time-domain (FDTD) method [24, 25] was used in [26] for a simulation-based study of the variation of path loss between patients, and the results indicated that path loss can vary up to a maximum of approximately 19% between patients, which affects the maximum 50% bit error rate in the system. A different approach was used to estimate the path loss in the body's channel for WCE with a set of X-ray CT images and measurements conducted at two different frequencies, i.e., 403 MHz and 2,450 MHz. The measurement results indicated that the radiation at 2,450 MHz was highly dependent on the medium and was attenuated to a greater extent [27]. In order to determine the path loss of the human body's communication channel in the abdominal region for a medically-implantable device, a numerical, electromagnetic (EM), simulation-

based statistical model was developed for 1–6 GHz and depths in the range of 10 to 150 mm [28].

However, in our research, the path loss of the human body's channel in electromagnetic wave propagation from the ingested capsule to the body's lead antenna in WCE was evaluated using the finite-integration technique and the heterogeneous body model. In order to indicate the optimum frequency of the system perfectly for the WCE, a wide range of frequencies was used in the simulation. The variation of path loss in different regions and depths in the GI path, considering actual human anatomy in the digital body model has been investigated extensively, but the results have not yet been published in the open literature.

## 2. METHOD AND ANALYSIS

The loss in electromagnetic wave propagation through free space can be determined easily from Equation (1), which indicates that the loss is a simple function of frequency and distance [29].

$$\text{Path loss} = P_t - P_r = 20 \log \frac{4\pi f d}{c} \tag{1}$$

where $P_t$ is the transmitted power, $P_r$ the received power, $d$ the distance between the transmitting and receiving points, $f$ the frequency, and $c$ the speed of light. Although it is possible to calculate the loss in wave propagation through a general lossy medium, it is quite difficult to do for the human body due to the complex and differing structures of the dielectric layer. In order to distinguish the different dielectric layers of the body from each other, an X-ray CT image was used in [27] to estimate the path loss by the body's channel. Using this method, the multi-layer human body can be converted to a single-layered, lossy medium with an average relative permittivity $\bar{\varepsilon}_r$ and conductivity $\bar{\sigma}$ in Equations (2) and (3), respectively:

$$\bar{\varepsilon}_r(f,p) = \frac{1}{N} \sum_{i=0}^{m} \varepsilon_{r_i} \cdot N_i(f,p) \tag{2}$$

$$\bar{\sigma}(f,p) = \frac{1}{N} \sum_{1=0}^{m} \sigma_i \cdot N_i(f,p) \tag{3}$$

where $\varepsilon_{r_i}$ and $\sigma_i$ are the relative permittivity and conductivity of the $i$th layer's tissue, respectively. $N_i$ is the number of pixels in the X-ray CT image of that layer, $p$ the set of directions from inside the body to outside the body, and $N$ the total number of pixels on the line of site from the source to the receiving antenna. Hence, the attenuation

constant [27, 30] of body tissue can be obtained from the values of $\bar{\varepsilon}_r$ and $\bar{\sigma}$ using Equation (4).

$$\alpha_{\text{body}} = \text{Re}\left[j\omega\sqrt{\mu\bar{\varepsilon}_r}\left(1 + \frac{\bar{\sigma}}{j\omega\bar{\varepsilon}_r}\right)\right] \tag{4}$$

Finally, the path loss by the body tissue $L_{\text{body}}$ was given by [31] as:

$$L_{\text{body}} = 20\log_{10}\exp\left(-\alpha_{\text{body}}d_{\text{body}}\right) \tag{5}$$

where $d_{\text{body}}$ is the distance between the source and the receiving antenna. However, this model only can provide a rough estimate of the path loss, which limits it applicability because more accurate estimates of path loss are required for simulations using the digital body model [30–37].

### 2.1. Human Body Model

The human body consist of multiple layers of tissue materials that have different dielectric properties. For modelling the human body's channel by simulating the electromagnetic fields, both the homogeneous and heterogeneous body models are used. Among these, the homogeneous body model is used more often in simulating EM fields because of its simplicity in that it contains only skin material and lossy material, such as salt water [38]. This body model was considered to be a good choice for observing radiation patterns, but the accuracy of its measurements of path loss measurement is suboptimal. In the heterogeneous body model, the complex, actual human anatomical structure exists as a voxel data set, which is more comparable to the human body for measuring path loss [39]. Also the different anatomical regions, such as the esophagus, stomach, and intestine, are distinguishable only in the heterogeneous model. This model consists of millions of small 'bricks' each of which has a different electrical property from the others, as is the case with actual body tissue. In order to achieve better accuracy, the heterogeneous digital body model (HUGO human body) was used in this work. The HUGO model of the human body that we used was a hypothetical male who was 187.4 cm tall, 37.4 cm wide and 34.1 cm deep (Figure 1). This model contained 32 different tissues with the highest resolution being $1 \times 1 \times 1\,\text{mm}^3$, allowing the simulation to produce more accurate results [40, 41]. The anatomical data, provided by the Visible Human Project of the U.S. National Institutes of Health, were implemented in HUGO model. The dielectric properties of the 32 distinct tissues were provided at seven different frequencies, ranging from 100 MHz to 2,450 MHz. The user interface of an integrated package in Microwave Studio gives the option of arbitrarily choosing whether to include or exclude any type of tissue

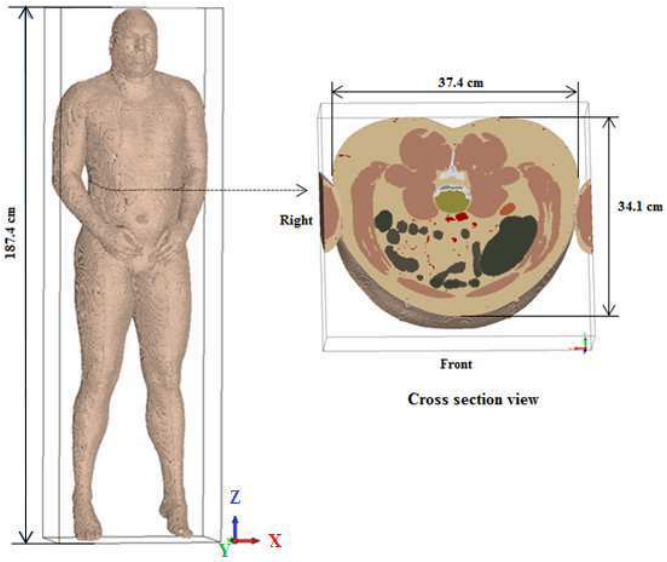


**Figure 1.** Heterogeneous model of the human body.

in the simulation. The frequency-dependent dielectric properties for the tissues used in this model are available in the data sheet of the Federal Communication Commission [45]. The conductivity of body tissue increases with frequency and consequence to high absorption loss [42, 43]. Likewise some of the tissues (fat, skin, muscle, blood, intestine) show high dissimilar dielectric property with each other that result high impedance mismatch and high reflection loss [44, 46, 47] at the interface of these layer.

## 2.2. Simulation Setup

In this simulation, the actual anatomical structure of the human body in a voxel data set was used [39], which allowed us to distinguish tissues and depths that were visually different from the surface of the body screen. The analogy of a typical WCE is shown in Figure 2(a). As can be seen in this figure, many different, practical locations of the capsule in the GI tract were considered to evaluate the path loss and its variation due to the different anatomical structures at different locations (Figure 2(b)). Table 1 shows the locations of the capsule that were assessed in the simulation. Rather than using the whole body, we used 10 cm $\times$ 10 cm $\times$ $D$ cm (varying)-shaped, sliced tissues from the selected locations and passed the EM signal through these

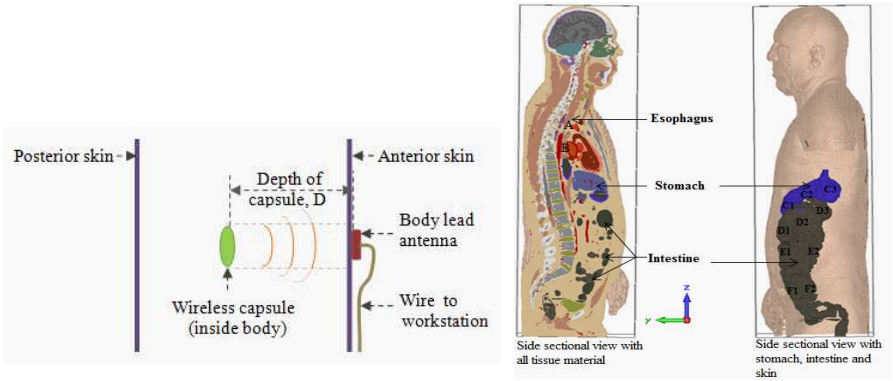


**Figure 2.** (a) Analogy of typical WCE; (b) human anatomy used in the body model showing the capsule locations that were considered in investigating path loss.

**Table 1.** Description of the capsule locations used in the investigation of path loss.

| Capsule location | Region | Depth from anterior skin ($D$ cm) |
|---|---|---|
| A | Upper Esophagus | 7 |
| B | Lower Esophagus | 13 |
| C1, C2, C3 | Stomach | 4, 10, 17 |
| D1, D2, D3 | Upper Intestine | 5, 10, 15 |
| E1, E2 | Intestine (above abdominal region) | 6, 14 |
| F1, F2 | Intestine (abdominal region) | 5, 10 |

tissues.

Two waveguide ports, i.e., port 1 (positive) and port 2 (negative), were used as a source and a receiving port, respectively. Port 1 set inside of the body and port 2 set outside of the body. The port 2, touching this port to the skin of the body will produce more accurate results. But both of the ports were set at a tissue-surface separation of 5 mm to adjust to the mesh-cell setting. Automatic, hexahedral, mesh generation was used because it was suggested in CST users' manual as the effective way to generate the mesh. The resultant path loss will be derived in between port 1 and port 2. This will include the effect of the interface between the skin and external medium-human body (air). The path loss for the 5 mm air gap (from outer skin to

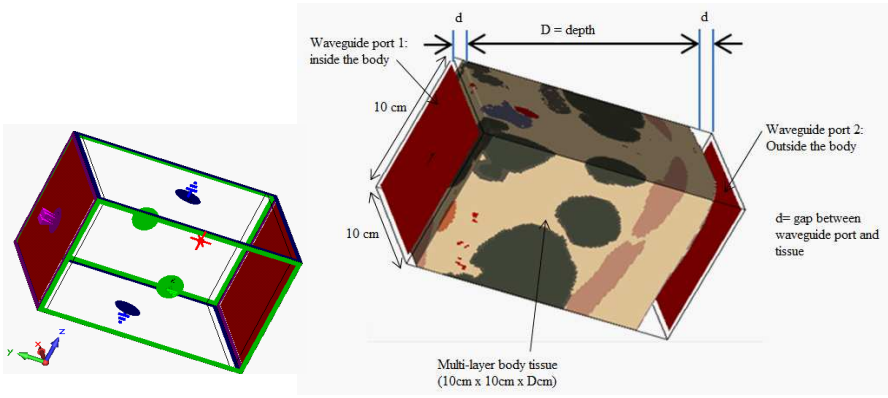


**Figure 3.** (a) Boundary condition; (b) simulation setup for investigating path loss in the body channel.

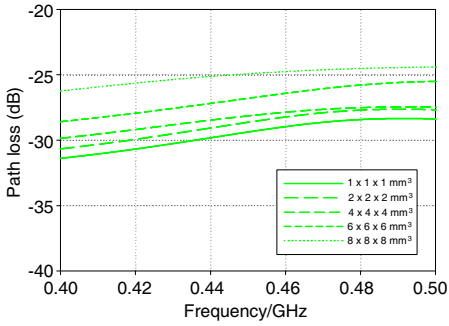


**Figure 4.** Variation of accuracy with the resolution of body model in simulation.

port 2) is too small and has been neglected. Figure 3 shows the simulation setup and boundary conditions used to investigate path loss. This simulation setup was based on that of a pyramidal microwave absorber [48–50]. The HUGO model can be used for seven different resolutions from $1 \times 1 \times 1$ mm$^3$ to $8 \times 8 \times 8$ mm$^3$ brick (pixel) size. Resolution used in simulation had a salient effect on the results, and this effect is shown in Figure 4. The figure shows that the results can vary by a maximum of 5 dB due to the selection of the maximum or the minimum resolution. In order to get more accurate results, the maximum resolution of $1 \times 1 \times 1$ mm$^3$ was used. In addition, the 32 distinct tissue materials that were available also were included to make the simulation more realistic.

## 3. RESULTS AND DISCUSSION

The results of path loss and its disparity (with capsule location) in the heterogeneous body channel were presented as a vertical bar graph and as a line graph. The vertical bar graph shows the path loss at different frequencies when the dielectric properties of the tissue was known (supplied by the vendor). In order to show how the path loss varied as a function of frequency, the path loss also was simulated and is represented by the line graph in the range of frequencies from 100 MHz to 2,450 MHz. The properties of the tissues over the range of frequencies that was used was based on the properties that are shown in Table 2.

**Table 2.** Frequency range that was considered in the simulation of the properties of specific tissue.

| Tissue property @ | Simulation range |
|---|---|
| 100 MHz | 100–350 MHz |
| 450 MHz | 350–750 MHz |
| 900 MHz | 750–1600 MHz |
| 1800 MHz | 1600–1850 MHz |
| 1900 MHz | 1850–2000 MHz |
| 2100 MHz | 2000–2300 MHz |
| 2450 MHz | 2300–2450 MHz |

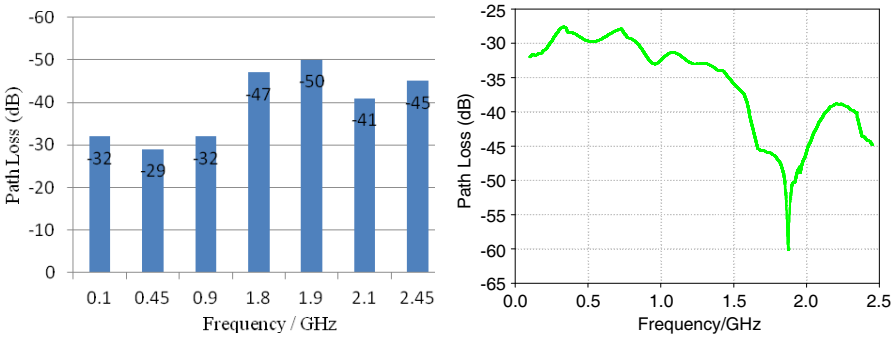


**Figure 5.** Path loss for the capsule position at A (upper esophagus): (a) with exact tissue property; (b) with the tissue property considered in Table 2.

As shown in Figures 5–10, the path loss was comparatively higher for frequencies greater than 900 MHz, irrespective of the location of the capsule. Due to this common characteristic of the body channel, it was recommended that frequencies less than 900 MHz be used for WCE [22, 51]. But the diverse, anatomical complexity affected the EM wave propagation differently in different regions of the anatomical structure. Consequently, the peak and nadir of path loss also varied depending on the location and depth of the capsule.

Figure 5 shows the path loss for the capsule location at A, the upper esophagus, where the line of sight distance between the capsule and the body lead antenna is 7 cm for body model that was used. At this location, the loss decreased from −32 dB at 100 MHz to −27 dB at 300 MHz and 700 MHz. The loss increased as the frequency increased above 700 MHz, and its peak was −60 dB between 1800 MHz and 1900 MHz (Figure 5(b)). Although the path loss decreased after 1900 MHz, it still remained at −45 dB at 2,450 MHz (Figure 5(a)), which is almost double the loss at 700 MHz. In the lower esophageal region, at capsule location B, overall path loss increased significantly compared to location A, due to the additional dielectric layers of the lungs, heart, and blood along the propagation direction that increased the reflection loss of the EM wave during propagation. When the capsule was in this position, path loss remained lower, i.e., less than −40 dB for frequencies less than 600 MHz. The peak loss increased to its maximum of −84 dB at 1,760 MHz, and the peak and nadir also shifted by about 100 MHz to lower frequencies (Figures 6(a) and 6(b)).

The variation of path loss over the frequency range was highly

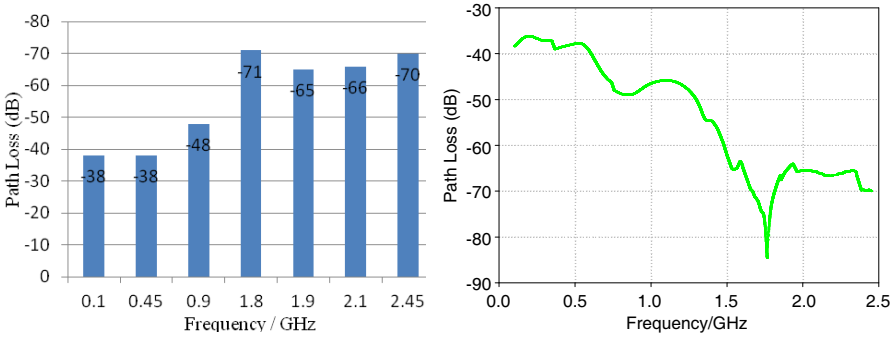


**Figure 6.** Path loss for the source position at B (lower esophagus): (a) with exact tissue property; (b) with the tissue property considered in Table 2.

related to the depth of the capsule in the body, and the variation increased as depth increased. Figure 7(a) shows that the differences between minimum and maximum losses were 20 dB, 31 dB, and 34 dB at C1 (at minimum depth, 4 cm), C2 (at centre depth, 10 cm), and C3 (at maximum depth, 17 cm), respectively. Figure 7(b) shows that there was a rapid decrease in path loss in the frequency range of 450 MHz to 900 MHz for the maximum and centre depths of the capsule in the stomach.

The intestine is the largest part of the human GI tract, and it consists of the most complex structure, with repetitive, curvy-shaped,

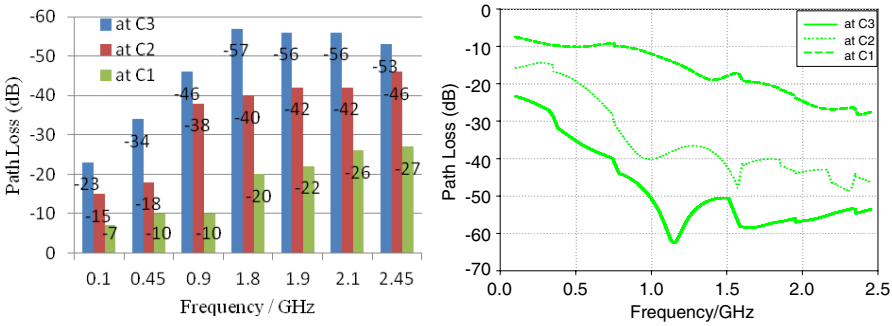


**Figure 7.** Path loss for the source position at C (stomach): (a) with exact tissue property; (b) with the tissue property considered in Table 2.

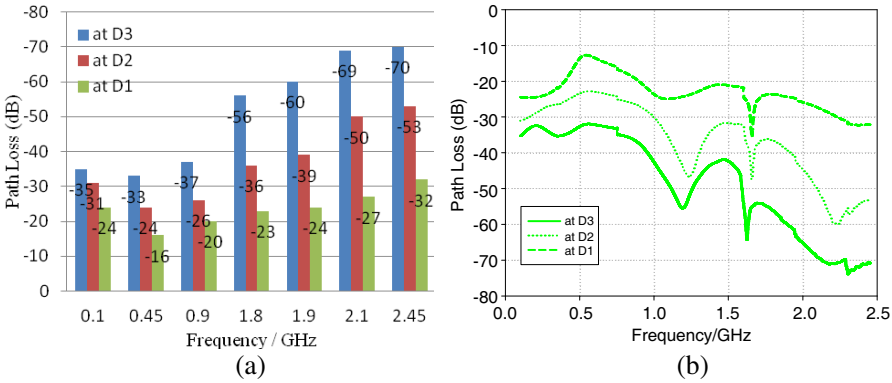


**Figure 8.** Path loss for the source position at D (upper intestine): (a) with exact tissue property; (b) with the tissue property considered in Table 2.

dissimilar tissue layers, while the anatomy of the stomach is not as hostile as that of the intestine for the propagation of EM waves. Because of these anatomical variations, the path loss is slightly greater in the intestine than in the stomach at equal depths of the capsule. Also, the number of dissimilar tissue layers differs in the upper and lower regions, which results in different propagation characteristics from the different locations in the intestine. At the upper portion of the intestine (location D), there is the greatest number of layers, whereas the lower portion around the abdomen increases the reflection loss and the absorption loss. Consequently, the overall loss in the upper portion of the intestine increases. Figures 8 and 10 show that the loss

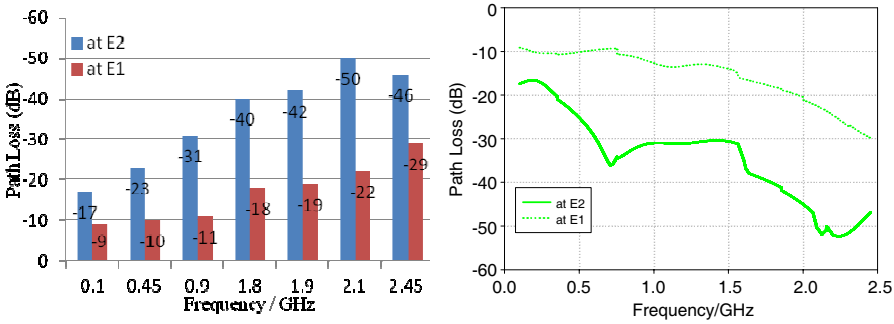


**Figure 9.** Path loss for the source position at E (upper abdominal region): (a) with exact tissue property; (b) with the tissue property considered in Table 2.

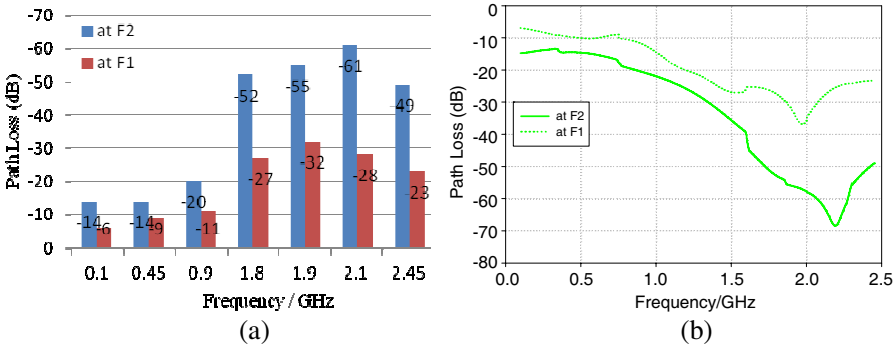


**Figure 10.** Path loss for the source position at F (abdominal region): (a) with exact tissue property; (b) with the tissue property considered in Table 2.

at the same frequency of 450 MHz and the same depth of 10 cm was −24 dB at D2 and −14 dB at F2. Figures 9 and 10 also show that the loss is greater in the upper abdominal region (E) than in the abdominal region (F).

At a frequency of 450 MHz, the maximum loss at E is −23 dB, while the maximum loss is −14 dB at F. In Figure 8(b), the path loss decreases at 500 MHz in the upper intestine and then continues to increase. But in Figures 9(b) and 10(b), the path loss increases continuously without a decrease in the upper abdominal and abdominal region. This indicates that the further the frequency is from 450 MHz, the greater the path loss becomes.

Finally, Table 3 shows the minimum and the maximum path loss when the capsule was in various anatomical locations. Clearly, there was a significant difference between these two losses. Also, the graphs show that this difference is even greater when the frequency is more than 900 MHz. Therefore, frequencies greater than 900 MHz are prohibited for WCE. But Table 3 shows that the minimum path loss

**Table 3.** Minimum and maximum path loss throughout the capsule's path.

| Location | Minimum Path loss (dB) | Maximum Path loss (dB) |
|---|---|---|
| A | −29 @ 450 MHz | −50 @ 1900 MHz |
| B | −38 @ 450 MHz | −71 @ 1800 MHz |
| C | −7 @ 100 MHz | −57 @ 1800 MHz |
| D | −16 @ 450 MHz | −70 @ 2450 MHz |
| E | −9 @ 100 MHz | −50 @ 2100 MHz |
| F | −6 @ 100 MHz | −61 @ 2100 MHz |

**Table 4.** Minimum and maximum path loss at frequencies of 450 MHz and 900 MHz.

| Location | 450 MHz | | 900 MHz | |
|---|---|---|---|---|
| | Minimum Path loss (dB) | Maximum path loss (dB) | Minimum Path loss (dB) | Maximum path loss (dB) |
| A | −29 | | −32 | |
| B | −38 | | −48 | |
| C | −10 | −34 | −10 | −46 |
| D | −16 | −33 | −20 | −37 |
| E | −10 | −23 | −11 | −31 |
| F | −9 | −14 | −11 | −20 |

always occurred at 450 MHz or lower. Also, Table 4 shows that the maximum path loss is 10 dB greater at 900 MHz than at 450 MHz. All of these results lead us to recommend the frequency of 450 MHz as the best choice for an optimized design of a telemetry system to be used in WCE.

## 4. CONCLUSIONS

The path loss in electromagnetic signal propagation through the human body's channel in wireless capsule endoscopy was investigated in this work. To relate to an actual human body more accurately, an heterogeneous digital body model was used, which was more suitable than a homogenous model, especially for the investigation of path loss. In our investigation, six vertical and a total of 12 different practical capsule positions were considered in the GI tract. The results showed that, for most of the cases, the path loss increased with frequency continuously. A slight decrease was observed at 500 MHz in the upper intestine and at 300 and 700 MHz in the upper esophagus region. The results led us to recommend the use of a frequency of 450 MHz for an efficient and effective capsule telemetry system. Although, the frequency range of 450 to 900 MHz has been suggested for WCE telemetry systems in some papers, it is clear from our results that the difference of the maximum path loss between 450 MHz and 900 MHz is 10 dB. Throughout the capsule's path, at the recommended frequency, the path loss varied between $-9$ dB and $-38$ dB. This variation is vital information because it is required in considering the link budget in the design of a high-efficiency telemetry system for next generation capsules with constant bit error rates as well as image transmission rate.

However, the upper and lower limits of the path-loss variations in this work are applicable only for the body model we used. It is unexpected to be significant dissimilarities with the subject similar fitness of used body model, but the upper and lower limits of path loss can vary with the patient's size, weight, gender, and age. To overcome this problem and to further optimize the WCE telemetry system, patient-specific telemetry systems must be designed and tested.

## ACKNOWLEDGMENT

The authors are grateful to the Ministry of Higher Education, Malaysia, for the financial support of this research work under the grant FRGS/FASA/TAHUN/SKK/JPP/03/6 via Politeknik Tuanku Syed Sirajuddin.

## REFERENCES


1. Iddan, G., G. Meron, A. Glukhovsky, and P. Swain, "Wireless capsule endoscopy," *Nature*, Vol. 405, 417, May 2000.
2. Yu, M., "M2A$^{TM}$ capsule endoscopy: A breakthrough diagnostic tool for small intestine imaging," *Gastroenterology Nursing*, Vol. 25, No. 1, 24–27, Feb. 2002.
3. Pan, G. and L. Wang, "Swallowable wireless capsule endoscopy: Progress and technical challenges," *Gastroenterology Research and Practice*, Vol. 2012, 1–9, 2011.
4. Theilmann, P., M. A. Tassoudji, E. H. Teague, D. F. Kimball, and P. M. Asbeck, "Computationally efficient model for UWB signal attenuation due to propagation in tissue for biomedical implants," *Progress In Electromagnetics Research B*, Vol. 38, 1–22, 2012.
5. Chen, Z. and Y.-P. Zhang, "Effects of antennas and propagation channels on synchronization performance of a pulse-based ultra-wideband radio system," *Progress In Electromagnetics Research*, Vol. 115, 95–112, 2011.
6. Phaebua, K., C. Phongcharoenpanich, M. Krairiksh, and T. Lertwiriyaprapa, "Path-loss prediction of radio wave propagation in an orchard by using modified UTD method," *Progress In Electromagnetics Research*, Vol. 128, 347–363, 2012.
7. Anang, K. A., P. B. Rapajic, R. Wu, L. Bello, and T. I. Eneh, "Cellular system information capacity change at higher frequencies due to propagation loss and system parameters," *Progress In Electromagnetics Research B*, Vol. 44, 191–221, 2012.
8. Anang, K. A., P. B. Rapajic, L. Bello, and R. Wu, "Sensitivity of cellular wireless network performance to system & propagation parameters at carrier frequencies greater than 2 GHz," *Progress In Electromagnetics Research B*, Vol. 40, 31–54, 2012.
9. Van Laethem, B., F. Quitin, F. Bellens, C. Oestges, and P. de Doncker, "Correlation for multi-frequency propagaton in urban environments," *Progress In Electromagnetics Research Letters*, Vol. 29, 151–156, 2012.
10. Vidal, N., S. Curto, J. M. Lopez-Villegas, J. Sieiro, and F. M. Ramos, "Detuning study of implantable antennas inside the human body," *Progress In Electromagnetics Research*, Vol. 124, 265–283, 2012.
11. Gao, Y., Y. Zheng, S. Diao, W. Toh, C. Ang, M. Je, and C. Heng, "Low-power ultrawideband wireless telemetry transceiver for medical sensor applications," *IEEE Transactions on Biomedical Engineering*, Vol. 58, No. 3, 768–772, Mar. 2011.

12. Diao, S., Y. Zheng, Y. Gao, C. Heng, and M. Je, "A 7.2 mW 15 Mbps ASK CMOS transmitter for ingestible capsule endoscopy," *2010 IEEE Asia Pacific Conference on Circuits and Systems (APCCAS)*, 512–515, 2010.
13. Chi, B., J. Yao, S. Han, X. Xie, G. Li, and Z. Wang, "Low-power, high-data-rate wireless endoscopy transceiver," *Microelectronics Journal*, Vol. 38, 1070–1081, 2007.
14. Kim, K., S. Yun, S. Lee, S. Nam, Y. Yoon, and C. Cheon, "A design of a high-speed and high-efficiency capsule endoscopy system," *IEEE Transactions on Biomedical Engineering*, Vol. 59, No. 4, 1005–1011, Apr. 2012.
15. Izdebski, P. M., H. Rajagopalan, and Y. Rahmat-Samii, "Conformal ingestible capsule antenna: A novel chandelier meandered design," *IEEE Transactions on Antennas and Propagation*, Vol. 57, No. 4, 900–909, Apr. 2009.
16. Zulkefli, M. S., F. Malek, M. H. Mat, S. H. Ronald, and M. F. Jamlos, "A compact peanut-shaped printed antenna for bio-telemetric tablet system," *2012 International Conference on Biomedical Engineering (ICoBE)*, 454–457, Feb. 27–28, 2012.
17. Gabriel, C., S. Gabriel, and E. Corthout, "The dielectric properties of biological tissues: I. Literature survey," *Physics in Medicine and Biology*, Vol. 41, 2231–2249, 1996.
18. Gabriel, S., R. W. Lau, and C. Gabriel, "The dielectric properties of biological tissues: II. Measurements in the frequency range of 10 Hz to 20 GHz," *Physics in Medicine and Biology*, Vol. 41, 2251–2269, 1996.
19. Gabriely, S., R. W. Lau, and C. Gabriel, "The dielectric properties of biological tissues: III. Parametric models for the dielectric spectrum of tissues," *Physics in Medicine and Biology*, Vol. 41, 2271–2293, 1996.
20. Ibrani, M., L. Ahma, E. Hamiti, and J. Haxhibeqiri, "Derivation of electromagnetic properties of child biological tissues at radio frequencies," *Progress In Electromagnetics Research Letters*, Vol. 25, 87–100, 2011.
21. Peyman, A., "Dielectric properties of tissues; variation with age and their relevance in exposure of children to electromagnetic fields; state of knowledge," *Progress in Biophysics and Molecular Biology*, Vol. 107, 434–438, 2011.
22. Chirwa, L. C., P. A. Hammond, S. Roy, and D. R. S. Cumming, "Electromagnetic radiation from ingested sources in the human intestine between 150 MHz and 1.2 GHz," *IEEE Transactions on Biomedical Engineering*, Vol. 50, No. 4, 484–492, Apr. 2003.

23. Jung, J. H., S. W. Kim, Y. S. Kim, and S. Y. Kim, "Electromagnetic propagation from the intestine-ingested source in the human body model," *IEEE Transactions on Antennas and Propagation*, Vol. 58, No. 5, 1683–1688, May 2010.
24. Vaccari, A., A. Cala' Lesina, L. Cristoforetti, and R. Pontalti, "Parallel implementation of a 3D subgridding FDTD algorithm for large simulations," *Progress In Electromagnetics Research*, Vol. 120, 263–292, 2011.
25. Guo, X.-M., Q.-X. Guo, W. Zhao, and W.-H. Yu, "Parallel FDTD simulation using NUMA acceleration technique," *Progress In Electromagnetics Research Letters*, Vol. 28, 1–8, 2012.
26. Abbasi, Q. H., A. Sani, A. Alomainy, and Y. Hao, "Numerical characterization and modeling of subject-specific ultrawideband body-centric radio channels and systems for healthcare applications," *IEEE Transactions on Information Technology in Biomedicine*, Vol. 16, No. 2, 221–227, Mar. 2012.
27. Takizawa, K., H. Hagiwara, and K. Hamaguchi, "Path-loss estimation of wireless channels in capsule endoscopy from X-ray CT images," *33rd Annual International Conference of the IEEE EMBS Boston*, 2242–2245, Massachusetts, USA, Aug. 30–Sep. 3, 2011.
28. Støa, S., R. Chavez-Santiago, and I. Balasingham, "An ultra wideband communication channel model for the human abdominal region," *2010 IEEE Globecom Workshops (GC Wkshps)*, 246–250, Dec. 6–10, 2010.
29. Katircioglu, O., H. Isel, O. Ceylan, F. Taraktas, and H. B. Yagci, "Comparing ray tracing, free space path loss and logarithmic distance path loss models in success of indoor localization with RSSI," *2011 19th Telecommunications Forum (TELFOR)*, 313–316, Nov. 22–24, 2011.
30. Pozer, D. M., *Microwave Engineering*, 3rd Edition, John Wiley & Sons, 2005.
31. Hall, P. S. and Y. Hao, *Antennas and Propagation for Body-centricwireless Communications*, Artech House, 2006.
32. Iero, D. A. M., T. Isernia, A. F. Morabito, I. Catapano, and L. Crocco, "Optimal constrained field focusing for hyperthermia cancer therapy: A feasibility assessment on realistic phantoms," *Progress In Electromagnetics Research*, Vol. 102, 125–141, 2010.
33. Mohsin, S. A., "Concentration of the specific absorption rate around deep brain stimulation electrodes during MRI," *Progress In Electromagnetics Research*, Vol. 121, 469–484, 2011.

34. Zhang, M. and A. Alden, "Calculation of whole-body SAR from a 100 MHz dipole antenna," *Progress In Electromagnetics Research*, Vol. 119, 133–153, 2011.
35. Kong, L.-Y., J. Wang, and W.-Y. Yin, "A novel dielectric conformal FDTD method for computing SAR distribution of the human body in a metallic cabin illuminated by an intentional electromagnetic pulse (IEMP)," *Progress In Electromagnetics Research*, Vol. 126, 355–373, 2012.
36. Ronald, S. H., M. F. B. A. Malek, S. I. Syed Hassan, E. M. Cheng, M. H. Mat, M. S. Zulkefli, and S. F. Maharimi, "Designing asian-sized hand model for SAR determination at GSM900/1800: Simulation part," *Progress In Electromagnetics Research*, Vol. 129, 439–467, 2012.
37. Vrbova, B. and J. Vrba, "Microwave thermotherapy in cancer treatment: Evaluation of homogeneity of SAR distribution," *Progress In Electromagnetics Research*, Vol. 129, 181–195, 2012.
38. Gemio, J., J. Parron, and J. Soler, "Human body effects on implantable antennas for ISM bands applications: Models comparison and propagation losses study," *Progress In Electromagnetics Research*, Vol. 110, 437–452, 2010.
39. Online Document AboutHUGO Human Body Model, available: www.sonnetsoftware.com/pdf/cst/human_body_and_radiator.pdf-d_radiator.pdf.
40. Gjonaj, E., M. Bartsch, M. Clemens, S. Schupp, and T. Weiland, "High-resolution human anatomy models for advanced electromagnetic field computations," *IEEE Transactions on Magnetics*, Vol. 38, No. 2, 357–360, Mar. 2002.
41. CST User Interface for Hugo Human Body Model, [online] available: http://www.cst.com/Content/Applications/Article /HUGO+Human+Body+Model.
42. Klemm, M. and G. Troester, "EM energy absorption in the human body tissues due to UWB antennas," *Progress In Electromagnetics Research*, Vol. 62, 261–280, 2006.
43. Moglie, F., V. Mariani Primiani, and A. P. Pastore, "Modeling of the human exposure inside a random plane wave field," *Progress In Electromagnetics Research B*, Vol. 29, 251–267, 2011.
44. Ott, H. W., *Electromagnetic Compatibility Engineering*, John Wiley & Sons, Inc., Hoboken, New Jersey, 2009.
45. Data sheet, Federal Communication Commission, [online], www.fcc.gov/fcc-bin/dielec.sh-09/2002.
46. Iqbal, M. N., M. F. B. A. Malek, S. H. Ronald, M. S. Bin Mezan,

K. M. Juni, and R. Chat, "A study of the EMC performance of a graded-impedance, microwave, rice-husk absorber," *Progress In Electromagnetics Research*, Vol. 131, 19–44, 2012.

47. Vidal, N., S. Curto, J. M. Lopez-Villegas, J. Sieiro, and F. M. Ramos, "Detuning study of implantable antennas inside the human body," *Progress In Electromagnetics Research*, Vol. 124, 265–283, 2012.
48. Malek, M. F. B. A., E. M. Cheng, O. Nadiah, H. Nornikman, M. Ahmed, M. Z. A. Abd Aziz, A. R. Osman, P. J. Soh, A. A. H. Azremi, A. Hasnain, and M. N. Taib, "Rubber tire dust-rice husk pyramidal microwave absorber," *Progress In Electromagnetics Research*, Vol. 117, 449–477, 2011.
49. Pues, H., Y. Arien, F. Demming-Janssen, and J. Dauwen, "Numerical evaluation of absorber reflectivity in an artificial waveguide," *2009 20th International Zurich Symposium on Electromagnetic Compatibility*, 409–412, Jan. 12–16, 2009.
50. Nornikman, H., M. F. B. A. Malek, P. J. Soh, A. A. H. Azremi, F. H. Wee, and A. Hasnain, "Parametric study of the pyramidal microwave absorber using rice husk," *Progress In Electromagnetics Research*, Vol. 104, 145–166, 2010.
51. Alomainy, A. and Y. Hao, "Modeling and characterization of biotelemetric radio channel from ingested implants considering organ contents," *IEEE Transactions on Antennas and Propagation*, Vol. 57, No. 4, 999–1005, Apr. 2009.